Journal of Medicinal Chemistry

Article

Discovery of a B-cell lymphoma 6 Protein–Protein Interaction Inhibitor by a Biophysics-driven Fragment-based Approach

Yusuke Kamada, Nozomu Sakai, Satoshi Sogabe, Koh Ida, Hideyuki Oki, Kotaro Sakamoto, Weston Lane, Gyorgy Snell, Motoo Iida, Yasuhiro Imaeda, Junichi Sakamoto, and Junji Matsui

J. Med. Chem., **Just Accepted Manuscript** • Publication Date (Web): 04 May 2017

Discovery of a B-cell lymphoma 6 Protein–Protein Interaction Inhibitor by a Biophysics-driven Fragment-based Approach

*Yusuke Kamada**[†], Nozomu Sakai**[†], Satoshi Sogabe[†], Koh Ida[†], Hideyuki Oki[†], Kotaro Sakamoto[†], Weston Lane[‡], Gyorgy Snell[‡], Motoo Iida[†], Yasuhiro Imaeda[†], Junichi Sakamoto[†] and Junji Matsui[†]*

[†]Takeda Pharmaceutical Company Limited, 26-1 Muraoka-Higashi 2-chome, Fujisawa, Kanagawa 251-8555, Japan

[‡]Takeda California Inc. 10410 Science Center Dr. San Diego CA 92121, USA

ABSTRACT: B-cell lymphoma 6 (BCL6) is a transcriptional factor that expresses in lymphocytes and regulates the differentiation and proliferation of lymphocytes. Therefore, BCL6 is a therapeutic target for auto-immune diseases and cancer treatment. This report presents the discovery of BCL6-corepressor interaction inhibitors by using a biophysics-driven fragment-based approach. Using the surface plasmon resonance (SPR)-based fragment screening, we successfully identified fragment **1** (SPR K_D = 1200 μM, ligand efficiency (LE) = 0.28), a competitive binder to the natural ligand BCoR peptide. Moreover, we elaborated **1** into the more potent compound **7** (SPR K_D = 0.078 μM, LE = 0.37, cell-free protein-protein interaction (PPI)

IC_{50} = 0.48 μM (ELISA), cellular PPI IC_{50} = 8.6 μM (M2H)) by a structure-based design and structural integration with a second high-throughput screening hit.

KEYWORDS: B-cell lymphoma 6, surface plasmon resonance, fragment-based drug discovery, fragment-assisted drug discovery, protein-protein interaction

INTRODUCTION

B-cell lymphoma 6 (BCL6) is a transcriptional factor that belongs to the bric-a-brac, tramtrack, broad complex/poxvirus zinc finger (BTB/POZ) family of proteins. It possesses BTB, RD2, and zinc finger domains, and interacts with three corepressors, i.e., BCoR, SMRT, and NCoR.[1] It drives germinal center B-cell formation and differentiation of T lymphocytes.[2-5] It is also involved in the differentiation and proliferation of diffuse large B-cell lymphomas.[6, 7] Consequently, it is thought to be an effective therapeutic target for the treatment of auto-immune diseases and cancer.

The crystal structure of the BCL6 BTB domain ($BCL6^{BTB}$) complexed with the SMRT peptide has already been reported.[8] The crystal structure of the co-complex with the BCL6 inhibitor 79-6 has also been solved.[9] These ligands bind in the lateral groove of the $BCL6^{BTB}$ homodimer. Parekh et al. have suggested that the lateral groove of the $BCL6^{BTB}$ homodimer could be an excellent therapeutic target to develop effective small-molecule inhibitors.[6] Several compounds and peptides, other than 79-6, have been reported as $BCL6^{BTB}$ inhibitors, including RI-BPI with a K_D of ~10 μM, Rifamycin SV with a K_D of ~1 mM, and FX1 with a K_D of 7 μM, all of which have binding affinities weaker than 1 μM (Figure 1).[10-12] Recently, we reported the peptide F1324, which inhibits the BCL6-BCoR interaction with a K_D of 0.57 nM (Figure 1).[13] Peptide F1324 also binds to the lateral groove of the $BCL6^{BTB}$ homodimer. These data suggest

that the lateral groove of the $BCL6^{BTB}$ homodimer could be a potent site for inhibitors to bind with high affinity.

Fragment-based drug discovery (FBDD) has been widely practiced in both industry and academia to identify compounds with good physiological profiles, new scaffolds, and new binding sites.[14, 15] The starting point of this approach is to identify molecule fragments with low affinity using high-concentration screening, and then to improve their affinity by linking or growing them.[16, 17] Biophysical assays (surface plasmon resonance (SPR), nuclear magnetic resonance (NMR), thermal shift assays, and so on) have been used for the FBDD approach because they are more sensitive than biochemical assays.[18, 19] Of these, SPR biosensing is the most cost-effective (low protein consumption and quick assay development) and provides high-content information on binding affinity and kinetics, and identification of pan-assay interference compounds (PAINS).[20, 21] Thus, SPR biosensing assays are often used for the FBDD approach.[22-25] Protein-protein interactions (PPIs) represent a challenging target for the biophysics-driven FBDD approach because the targets, like BCL6, do not possess a deep binding pocket.[26-29]

In this study, SPR-based fragment screening was performed against BCL6 to discover BCL6-cofactor interaction inhibitors. As a result, we successfully identified triazine fragment **1**, which binds to the lateral groove of the $BCL6^{BTB}$ homodimer where BCoR also binds. Furthermore, fragment **1** was optimized into the more potent inhibitor **7**, which exhibits cellular activity and two-digit nanomolar binding affinity, by structure-based drug design using X-ray analysis and structural integration with a second high-throughput screening (HTS) hit. This process represents a highly successful fragment-assisted drug discovery approach (FADD).[30, 31]

RESULTS AND DISCUSION

Protein preparation. To identify BCL6 inhibitors that disrupt the interaction between BCL6 and cofactors, we attempted to prepare $BCL6^{BTB}$ cofactors that bind to the lateral groove of the $BCL6^{BTB}$ homodimer. $BCL6^{BTB}$ is approximately 15 kDa in size, but despite its small size, its domain contains five cysteine residues. We speculated that the high proportion of Cys residues would cause instability, which was reinforced by the fact that the co-crystal structure of $BCL6^{BTB}$ has been obtained using the Cys-mutant (Ala5-Glu129, C8Q, C67R, and C84N) to prevent aggregation.[8] In addition, we needed to consider that the high concentration (mM) required for SPR screening can cause false positives. In an attempt to mitigate this tendency for false positives, we decided to use the Cys-mutation protein for SPR-based screening.

SPR assay development. For our SPR-based screening, we used a Biacore 4000 high-throughput instrument with five detection areas for protein immobilization and four flow cells for compound injection. This parallel immobilization enables the evaluation of selectivity and nonspecific binding simultaneously.[32-34] We also screened against both wild type (wt) and mutant (mt) $BCL6^{BTB}$ by SPR. Figures 2A and 2B show the layout of the sensor chip used in this screening. Avi-tagged wt $BCL6^{BTB}$ and avi-tagged mt $BCL6^{BTB}$ were captured onto spot 1 and spot 2, respectively, by NeutrAvidin. In addition, wt $BCL6^{BTB}$ was covalently immobilized onto spot 5 by an amine coupling reaction (Figure S1). This configuration enabled us to evaluate binding to captured wt $BCL6^{BTB}$, captured mt $BCL6^{BTB}$, coupled wt $BCL6^{BTB}$, and coupled NeutrAvidin.

To verify the activity of each immobilized $BCL6^{BTB}$, we evaluated the binding of the BCoR peptide as a positive control (Figures 2C to 2F). The BCoR peptide successfully binds with each $BCL6^{BTB}$ in a dose-dependent manner. The K_D values for the BCoR peptide with each $BCL6^{BTB}$ are in the two-digit micromolar range. Since there are no significant differences in the binding

affinities among the different $BCL6^{BTB}$s, the mutation of the Cys residues is not thought to affect the interaction between BCL6 and BCoR, and we concluded that each $BCL6^{BTB}$ is immobilized while retaining its activity.

For performing high-quality SPR-based screening, maintaining the stability of the immobilized protein is important.[35-37] Therefore, selection of a suitable buffer is critical to retain stability. Compared with that used in biochemical assays, the concentration of dimethyl sulfoxide (DMSO) required for SPR-based screening is generally higher to solubilize the fragments at high concentration. Accordingly, the influence of DMSO on the activities of the immobilized $BCL6^{BTB}$s was evaluated (Table 1 and Figure S2). The K_D and R_{max} values for the BCoR peptide are unaffected by the concentration of DMSO. Moreover both wt $BCL6^{BTB}$ and mt $BCL6^{BTB}$ are stable for 36 h (500 injections) under buffer conditions of 1% or 5% DMSO. Therefore, we decided to perform screening with a 5% DMSO buffer to ensure a 1 mM solubility for the fragments.

Primary fragment screening. In a primary SPR-based screening of our in-house fragment library, we were able to obtain the screening data for captured wt $BCL6^{BTB}$, captured mt $BCL6^{BTB}$, coupled wt $BCL6^{BTB}$, and NeutrAvidin simultaneously using the Biacore 4000 apparatus. In the screening with the captured mt $BCL6^{BTB}$, the sensorgrams against most of the fragments show a reasonable box-shape, indicating fast binding (Figure 3B). Conversely, captured wt $BCL6^{BTB}$ presents many plots that indicate slow binding (Figure 3A). These data suggest that many fragments reversibly reacted with the Cys residues on wt BCL6 due to a concentration as high as 1 mM. Regarding the immobilization method, the binding responses of the positive control (BCoR) to coupled wt $BCL6^{BTB}$ decrease depending on the injection number,

while the binding responses of the positive control to each captured $BCL6^{BTB}$ are stable (Figures 3A to 3C). These results indicate that captured mt $BCL6^{BTB}$ is optimal for stable screening.

In the primary screening, we identified 266 fragments for captured wt $BCL6^{BTB}$, 256 fragments for captured mt $BCL6^{BTB}$, 273 fragments for coupled wt $BCL6^{BTB}$, and 50 fragments for NeutrAvidin. The Venn diagram in Figure 2E summarizes the results of this fragment screening. A total of 64 compounds bind to all the $BCL6^{BTB}$s, hence these fragments were selected as the first priority for the follow-up dose-response tests.

Discovery and characterization of fragment 1. To confirm the reproducibility and dose-responsivity of the 64 fragments, we performed dose-titration experiments. All the fragments show binding responses in a dose-dependent and reversible manner (data not shown). Next, we performed saturation transfer difference-nuclear magnetic resonance (STD-NMR) experiments to prioritize the 64 fragments. Seven out of the 64 fragments exhibit binding to BCL6 (data not shown). Of seven binding fragments, we focused on fragment **1** (Figure 4A), which shows binding to BCL6 by STD-NMR (Figure 4B) and furthermore competition with the BCoR peptide by SPR competition experiments (Figure 4C). The K_D value for **1** was determined to be 1.2 mM by SPR, and its ligand efficiency (LE) was calculated to be 0.28 from its K_D value. An LE of at least 0.29 is necessary to develop an orally available candidate.[38] Therefore, **1** is a good starting point for elaboration into potent BCL6 inhibitors.

For further optimization of fragment **1**, we attempted to determine its binding mode by determining the co-crystal structure of **1** with wt $BCL6^{BTB}$. Co-crystals of **1** with $BCL6^{BTB}$ were obtained by soaking into unliganded $BCL6^{BTB}$ crystals in which the biological homodimer is related by crystallographic 2-fold symmetry. Electron density indicated that **1** binds to the lateral

groove at the dimer interface and exhibits alternate conformations of the aminotriazine moiety (Figures 4 and S4). The linker nitrogen forms a hydrogen bond with the main-chain oxygen of Met51. Comparison with the binding mode of 79-6 shows that **1** occupies the same site with a similar interaction pattern (data not shown). Therefore, we evaluated the BCL6 binding affinities of several pyrimidine derivatives that are structurally related to **1**.

Structure-activity relationships of compounds related to fragment 1. Table 2 summarizes the structure-activity relationships of the pyrimidine derivatives along with the original fragment **1**. Pyrimidine derivative **2** exhibits a weak binding potency (K_D = 3000 μM), while the introduction of fluorine (**3**) or chlorine (**4**) atoms onto the 5-position of compound **2** results in significantly improved binding affinities (K_D = 180 and 68 μM, respectively). Chloropyrimidine **4** exhibits good LE (0.38), and may be a promising compound for further optimization with the aim to develop more potent BCL6 inhibitors.

Structural integration with a second HTS hit. Simultaneously, an independent HTS campaign for BCL6 inhibitors identified the weak BCL6 inhibitor **5** (K_D = 88 μM, LE = 0.16), which also has a pyrimidine core structure, as shown in Figure 5; compound **5** was discovered by the HTS campaign using the ELISA assay monitoring the interaction between the $BCL6^{BTB}$ and the BCoR peptide. The structural resemblance of **5** to **4** prompted us to integrate these two structures, forming the "hybrid compounds" shown in Figure 5. Co-crystal structure determination of compounds **4** and **5** with $BCL6^{BTB}$ confirmed that these compounds exhibit the same binding modes as that of the initial triazine fragment **1** (Figures 6 and S4). As expected, the two aromatic rings connected by the amine linker in the two structures significantly overlap. The co-crystal structure of **4** reveals that the chlorine atom at the 5-position of the pyrimidine core occupies a small lipophilic region of $BCL6^{BTB}$. The binding mode information of the HTS-

derived pyrimidine derivative **5** shows that the carbonyl oxygen of the right-hand-side cyclic amide moiety interacts with Glu115 of $BCL6^{BTB}$. Therefore, based on the structural superposition of **5** with **4**, the hybrid compounds **6** and **7** were designed and synthesized (Table 3). We selected a simple unsubstituted pyridinylmethyl substituent for compound **7** while taking synthetic tractability into account.

The pyrimidine derivatives **6** and **7** exhibit significantly improved BCL6 binding affinities (K_D = 9.3 and 0.078 μM, respectively) compared to those of the fragment derivative **4** and HTS hit **5**. To confirm the binding modes, the co-crystal structures of compounds **6** and **7** were determined, as well as those of the other compounds (Figures 7A and S4). The electron density map shows that the pyridine moiety of compound **7** is exposed to solvent and mostly disordered. Both compounds bind to $BCL6^{BTB}$ in the same binding mode as those for compounds **1**, **4**, and **5**. The linker nitrogen forms a hydrogen bond with the main-chain oxygen of Met51, and the carbonyl oxygen of the cyclic amide moiety interacts with Glu115. The reasons for the significant improvement in binding affinity by introduction of the pyrimidine ring are unclear because no specific structural features are observed.

As compound **7** exhibits two-digit nanomolar binding affinity along with good LE (0.37), we also evaluated the BCL6-BCoR PPI inhibitory activity of **7** in cell-free and cellular assays (Figures 7B to 7E). To evaluate the PPI inhibitory activities in cells, previously reported M2H assay was used.[13] Briefly, HEK293T cells were transfected with the GAL4-responsive reporter plasmid, the bait expression plasmid (GAL4 DNA-binding domain fused to wt BCL6, Ala5-Glu129), and the VB expression plasmid (VP16 activation domain fused to BCoR, Leu112-Ala753). Then, the PPI activities were evaluated by monitoring luciferase activities in the transfected HEK293 cell lysates. Compound **7** exhibits potent cell-free PPI inhibitory activity

(ELISA IC_{50} = 0.48 μM) along with moderate cellular potency (M2H IC_{50} = 8.6 μM). Taken together, compound **7** is a promising BCL6 inhibitor candidate for further exploration. The total process of the fragment-based approach was summarized in Figure 8. Scaffold hopping of the initial triazine fragment yielded the pyrimidine fragment **2**, which enabled an introduction of a substituent occupying the small lipophilic region of $BCL6^{BTB}$. Structure-based modification of the resulting compound **4** along with the consolidation of HTS hit **5** led to the discovery of the cell-active compound **7**. The HTS hit **5** had a poor ligand efficiency (LE = 0.16), and its complex chemical structure made its modification rather difficult. Conversely, the fragment-derived compound **4** was a very good step for further modification due to its good ligand efficiency (LE = 0.38) and small molecular size.

CHEMISTRY

Synthetic methods for pyrimidine derivatives are shown in Scheme 1. The reaction of the 4-chloropyrimidines **8**–**11** with anilines **12** and **13** give the corresponding 4-anilinopyrimidines **2**, **6**, **14**, **15**, and **16**. Amination of **14**–**16** with amines **17** and **18** at the 2-position of the pyrimidine derivatives gives the di- or tri-substituted pyrimidine derivatives **3**, **4**, and **7**.

CONCLUSIONS

To identify novel and promising starting points for the discovery of potent BCL6 inhibitors, we adopted an FBDD approach, which represents a challenge given that the target is a PPI. We identified 64 novel binding fragments using SPR-based fragment screening, and among them, fragment **1** showed moderate LE (0.28) and competition with the BCoR peptide. Moreover, BCL6 binding affinities of several structurally related pyrimidine derivatives were also measured, and we identified the more potent fragment-like pyrimidine derivative **4** (K_D = 68 μM).

Consolidation of the structural information of compound **4** with the independently obtained HTS hit **5** led to the identification of the potent BCL6 inhibitor **7** (K_D = 0.078 μM, LE = 0.37), which is >15,000-fold more potent than the initial fragment **1**. Compound **7** also exhibited an efficacy in cell-free and cellular PPI assays (ELISA IC_{50} = 480 nM, M2H IC_{50} = 8.6 μM). These findings suggest that the combination of biophysics-driven FBDD, SBDD, and FADD is a promising strategy for hit identification and lead generation against challenging targets such as PPIs.

EXPERIMENTAL SECTION

Preparation of BCL6. The fragments of His, avi, SUMO (LifeSensors), Flag, Tobacco Etch Virus (TEV) protease recognition sequence, and $BCL6^{BTB}$ (human BCL6 from 5 to 129 aa) were amplified by the polymerase chain reaction (PCR) and ligated into pET21 vector (Merck). The mt $BCL6^{BTB}$ (C8Q, C67R, C84N) was constructed by the overlap PCR method. The proteins were expressed in *E. coli* BL21 (DE3) (NIPPON GENE) and partially biotinylated on avi-tag by endogenous BirA. The proteins were purified using Ni-NTA (QIAGEN) and Superdex200 (GE healthcare) columns. For Flag-tagged wt $BCL6^{BTB}$, SUMO was digested by ULP1 (LifeSensors). To remove ULP1, His-avi-SUMO, and uncleaved protein, the digested solution was passed through an Ni-NTA column in 50 mM Tris-HCl pH 8.0, 300 mM NaCl, 5% glycerol, and 1 mM DTT. To increase the purity, ion-exchange chromatography (monoQ, GE Healthcare) was conducted. The purified proteins were concentrated to 2 mg/ml for storage at −80°C.

Fragment library. The library contained 1494 fragments. All fragments in the library had a clogP <3.5, the number of H-bond acceptors and donors were <6 and <3 respectively, and rotatable bonds were <3. Heavy atom count ranged between 8 and 15. The molecular weight of

the fragments were <350 Da (average 180 Da), and the average of the aromatic rings was 1.5. Fragments were dissolved at 200 mM in 100% DMSO and stored at −30 °C.

SPR. SPR biosensing experiments were performed at 22°C on Biacore 4000 and Biacore S200 instruments equipped with SeriesS CM5 and SA sensor chips (GE healthcare).

HBS-P+ (10 mM Hepes pH 7.4, 150 mM NaCl, 0.05% Surfactant P20, GE healthcare) supplemented with 1 mM DTT was used as the running buffer for immobilization. NeutrAvidin (Thermo Fisher Scientific Inc.) was covalently coupled onto spots 1, 2, and 3 of a CM5 sensor chip following the standard amine coupling procedure according to the manufacturer's instructions. Typical immobilization levels of NeutrAvidin ranged from 10,000 to 13,000 resonance units (RUs). Subsequently, avi-tagged wt $BCL6^{BTB}$ and avi-tagged mt $BCL6^{BTB}$ were injected to spots 1 and 2, respectively. The surfaces were blocked by injecting biocytin (Thermofisher) to spots 1, 2, and 3. Approximately 13,000 RUs of each $BCL6^{BTB}$ were captured by NeutrAvidin. Furthermore, wt $BCL6^{BTB}$ was immobilized on spot 5 via the standard amine coupling procedure, resulting in immobilization levels of around 4,000 RUs.

For the interaction studies, binding experiments were performed in 20 mM Tris, pH 8.0, 150 mM NaCl, 0.01% Surfactant P20, 1 mM DTT, and 5% DMSO. Different concentration sample solutions were injected for 30 or 60 s at a flow rate of 30 or 50 μL/min and the dissociation was thereafter followed for up to 30, 60, or 150 s. Data processing and analysis were performed using the Biacore 4000 and Biacore S200 evaluation software (GE healthcare). Solvent correction was included as described in the Biacore software handbook. Sensorgrams were double referenced prior to fitting the concentration series to a steady-state affinity model. The dissociation constant K_D was calculated using the equation below.

$$K_D = R_{max} \times C/R - C$$

where R_{max}, R, and C correspond to the sample binding capacity of the surface (RU), the normalized response of test sample (RU), and the concentration of the test solution (M), respectively. LE was calculated using the equation below.

$$LE = \Delta G/HA = (-2.303 \times R \times T) \times \log (K_D)/HA$$

where ΔG, HA, R, and T correspond to the Gibbs free energy (kcal/mol), heavy atom count, the ideal gas constant (1.987×10^{-3} kcal/K/mol) and the temperature in Kelvin (K).[39]

For the primary screen, Takeda's fragment library were diluted to 1 mM in the running buffer and injected for 30 s. Then, the dissociation was followed for 30 s. Every 33rd cycle, a positive control containing 100 μM BCoR peptide ((Arg498-Pro514)-Lys, Acetyl-RSEIISTAPSSWVVPPK-OH, chemically synthesized by Toray Research Center) and running buffer as a blank were injected. Data processing and analysis were performed using the Biacore 4000 evaluation software. Solvent correction was included as described in the Biacore 4000 software handbook. The binding responses were normalized by the positive control and the molecular weight of each sample. Fragments with a normalized binding response that exceeded median + median absolute deviation were selected as primary hits. As for NeutrAvidin, fragments with a normalized response that was more than 90% against their theoretical R_{max} were selected.

For competition studies, data were acquired for test compounds binding to BCL6 in the presence of 100 μM BCoR peptide in the running buffer and samples. When a compound binds to the same site as the BCoR peptide, the response for the compound decreases.[40]

X-ray Crystallography. Crystals of unliganded $BCL6^{BTB}$ for soaking experiments were obtained as described previously.[13] Crystallization was by vapor-diffusion using the sitting-drop method from 0.1 M Bis-Tris pH 6.5, 0.7 M potassium/sodium tartrate at 20°C. To generate protein-ligand complexes, crystals were typically soaked for 2 h in a reservoir solution containing 1 mM ligand(s). Prior to data collection, crystals were immersed in the reservoir solution with the addition of 30% glycerol as a cryoprotectant, and were flash-frozen in liquid nitrogen. Diffraction data were collected from a single crystal using the CCD detector Quantum 315 (ADSC) at beamlines 5.0.2 and 5.0.3 of the Advanced Light Source (Berkeley) under a 100 K nitrogen cryostream. The data were reduced and scaled with HKL2000.[41] The structures were solved by the molecular replacement method with Molrep[42] of the CCP4 software suite[43] using the $BCL6^{BTB}$ structure (PDB code: 1R28) as a search model. The structures were refined through an iterative procedure utilizing REFMAC[44] followed by model building in COOT.[45] The final models were validated using Molprobity.[46] Crystallographic processing and refinement statistics are summarized in Table S1. All structural figures were generated using PyMOL (Schrödinger).

STD-NMR. ^{1}H NMR spectra were recorded using a 3 mm NMR tube on a 600 MHz Avance spectrometer (Bruker Biospin) equipped with a 5 mm TCI cryoprobe. All NMR samples were prepared in 50 mM phosphate D_2O buffer at pH 7.4 containing 150 mM NaCl, 1 mM DTT-d_{10}, and 0.2% DMSO-d_6 in D_2O solvent. The STD spectrum was acquired from a sample containing 400 μM fragment **1** and 20 μM $BCL6^{BTB}$ at 15°C with 32 scans with on- and off-resonance saturation frequencies of 0.4 ppm and 30 ppm, respectively, and a total saturation time of 2.0 s. The decrease in signal intensity for on-resonance irradiation results from the transfer of saturation from $BCL6^{BTB}$ to fragment **1**. The STD spectrum of fragment **1** was obtained by

subtracting the on-resonance spectrum from the off-resonance spectrum. A positive signal in the STD spectrum indicates binding of fragment **1** to $BCL6^{BTB}$.

ELISA. Biotinylation of the ε-amino group of the C-terminus Lys on the BCoR peptide was carried out with the Biotin-$(AC_5)_2$ Sulfo-OSu (DOJINDO) according to the protocol recommended by the manufacturer. The wells of a Nunc Maxisorp microplate (460-518) were coated with streptavidin (SA) (Wako) and were blocked with phosphate-buffered saline (PBS) that contained 1.0% Casein. The biotinylated BCoR peptide was captured by the SA, and a wt $BCL6^{BTB}$ (0.5 nM) solution in PBS that contained 0.05% Tween20 and 1 mM DTT (PBST) was added to the wells. After washing with PBST, bound $BCL6^{BTB}$ was detected using horseradish peroxidase (HRP)-conjugated anti-FLAG antibody (Sigma). The amounts of HRP in the wells were measured using a chemical luminescent regent (Thermo Fisher Scientific Inc.).[13] Percent inhibition was calculated based on wells without $BCL6^{BTB}$ as a high control and without compound as a low control.

M2H. The assay was performed according to a procedure described previously.[1] The vectors pGL4.35, pBind, and pACT were obtained from Promega Corp. As template DNA, human BCL6 cDNA was isolated by PCR from a human skeletal muscle cDNA library (TAKARA Bio) and human BCoR cDNA was purchased from GeneCopoeia Inc. Each cDNA fragment was granted a restriction site by PCR and digested with restriction enzymes to insert into pBIND or pACT, respectively. M2H was performed in HEK293T cells that were transfected with the reporter constructs pGL4.35 containing GAL4 special response element of firefly luciferase (9×GAL4UAS); pBIND/GAL4-BCL6 (Ala5–Glu129); and pACT/VP16-BCoR (Leu112–Ala753) by Fugene HD (Promega). The transfected cells were seeded at 1×10^4 cells/15 μL/well on 384-well plates (CORNNING) in Dulbecco's modified Eagle's medium that contained 10%

fetal bovine serum. After incubation for 20 h at 37°C under 5% CO_2, cells were lysed to measure luciferase activity using the Bright-Glo luciferase assay system (Promega).[13] Percent inhibition was calculated based on the well without transfection of pBIND/GAL-BCL6 (Ala5–Glu129) as the high control and the well without the compound as a low control.

Chemistry. ^{1}H NMR spectra were obtained on a Bruker AVANCE II (300 MHz) spectrometer. Chemical shifts for ^{1}H NMR are reported in parts per million (ppm) downfield from tetramethylsilane (δ) as an internal standard in deuterated solvent, and the coupling constants (*J*) are given in hertz (Hz). The following abbreviations are used for spin multiplicity: s = singlet, d = doublet, t = triplet, q = quartet, dd = doublet of doublets, dt = doublet of triplets, m = multiplet, and brs = broad singlet. Reaction progress was monitored by thin-layer chromatography (TLC) analysis on silica gel 60 F_{254} plates (Merck) or an NH TLC plate (Fuji Silysia Chemical Ltd.). Column chromatography was carried out on a silica gel column (Chromatorex® NH-DM1020, 100–200 mesh; Fuji Silysia Chemical, Ltd.) or on Purif-Pack (SI ϕ 60 μM or NH ϕ 60 μM; Fuji Silysia Chemical, Ltd.). Preparative HPLC (prep-HPLC) purification was performed on a Waters 2525 equipped with a L-column2 ODS (20 × 150 mm i.d., 5 μm particle size, CERI, Japan), eluting with 0.1% TFA in distilled water (Mobile phase A) and 0.1% TFA in acetonitrile (Mobile phase B) using the following elution gradient: 20% B to 55% B over 7 min followed by 100% B isocratic over 4 min at a flow rate of 20 mL/min. The products were detected by monitoring the mass spectra recorded using a Waters ZQ2000 with electrospray ionization. The purity of all compounds used in biological studies was determined to be ≥95% by elemental analysis or HPLC-MS analysis. Low-resolution mass spectra were acquired using a Shimadzu UFLC/MS (Shimazu LC-20AD/LCMS-2020) in electron spray ionization mode (ESI+). The column used was an L-column 2 ODS (3.0 × 50 mm i.d., 3 μm;

CERI, Japan) at a temperature of 40°C and a flow rate of 1.2 or 1.5 mL/min. Condition 1: Mobile phases A and B under acidic conditions were 0.05% TFA in water and 0.05% TFA in MeCN, respectively. The proportion of mobile phase B was increased linearly from 5% to 90% over 0.9 min, and maintained at 90% over the next 1.1 min. Condition 2: Mobile phases A and B under neutral conditions were a mixture of 5 mmol/L $AcONH_4$ and MeCN (9:1, *v/v*) and a mixture of 5 mmol/L $AcONH_4$ and MeCN (1:9, *v/v*), respectively. The proportion of mobile phase B was increased linearly from 5% to 90% over 0.9 min, and maintained at 90% over the next 1.1 min. Elemental analyzes were carried out by Sumika Chemical Analysis Service, Ltd. All commercially available solvents and reagents were used without further purification. Yields were not optimized. Compounds **1** and **5** are commercially available.

***N*^{4}-Phenylpyrimidine-2,4-diamine (2).** A mixture of 4-chloropyrimidin-2-amine (100 mg, 0.77 mmol), aniline (108 mg, 1.16 mmol), and conc. HCl (1 drop) in *i*-PrOH (1.0 mL) was heated at 80°C for 2 h. The reaction mixture was diluted with saturated aqueous $NaHCO_3$ solution and extracted with EtOAc. The organic layer was concentrated, and the residue was purified by column chromatography (NH silica gel, eluted with 50% to 100% EtOAc in hexane). The desired fractions were concentrated, and the residue was triturated with hexane-EtOAc to give compound **2** (98 mg, 69%) as an off-white solid. ^{1}H NMR (DMSO-d_6) δ 6.00 (1H, brs), 6.20 (2H, brs), 6.94 (1H, brs), 7.27 (2H, brs), 7.53–8.00 (3H, m), 9.08 (1H, brs). MS *m*/*z* 187.1 $(M+H)^+$. Anal. Calcd for $C_{10}H_{10}N_4$: C, 64.50; H, 5.41; N, 30.09. Found: C, 64.30; H, 5.56; N, 30.21.

5-Fluoro-*N*^{4}-phenylpyrimidine-2,4-diamine (3). A mixture of compound **14** (63 mg, 0.28 mmol) and 28% aqueous ammonia solution (2.5 mL, 37.2 mmol) in *i*-PrOH (2.5 mL) was heated at 150°C under microwave irradiation for 4 h. The reaction mixture was concentrated, and the

residue was purified by prep-HPLC. The desired fraction was concentrated and neutralized with saturated aqueous $NaHCO_3$ solution. The precipitated solid was collected, washed with H_2O and IPE, air-dried, and dried *in vacuo* to give **3** (9.1 mg, 16%) as a colorless solid. ^{1}H NMR (DMSO-d_6) δ 6.18 (2H, s), 7.01 (1H, t, J = 7.1 Hz), 7.28 (2H, t, J = 7.7 Hz), 7.80–7.89 (3H, m), 9.04 (1H, s). MS m/z 205.1 $(M+H)^+$. Anal. Calcd for $C_{10}H_9FN_4 \cdot 0.1\ H_2O$: C, 58.30; H, 4.50; N, 27.20. Found: C, 58.33; H, 4.67; N, 27.32.

5-Chloro-N^4-phenylpyrimidine-2,4-diamine (4). A mixture of **15** (100 mg, 0.42 mmol) and 2 M ammonia *i*-PrOH solution (5.0 mL, 10 mmol) was heated at 150°C under microwave irradiation for 4 h. The reaction mixture was concentrated, and the residue was purified by prep-HPLC. The desired fraction was concentrated and neutralized with saturated aqueous $NaHCO_3$ solution. The precipitated solids were collected, washed with H_2O and IPE, and dried *in vacuo* to give **4** (23 mg, 25%) as an off-white solid. ^{1}H NMR (DMSO-d_6) δ 6.41 (2H, s), 7.01–7.08 (1H, m), 7.26–7.33 (2H, m), 7.74 (2H, d, J = 8.1 Hz), 7.91 (1H, s), 8.45 (1H, s); MS m/z 221.1 $(M+H)^+$. HPLC analysis conditions 1: R_t = 0.65 min (100% purity); 2: R_t = 0.89 min (100% purity).

5-((5-Chloropyrimidin-4-yl)amino)-1,3-dihydro-2*H*-indol-2-one (6). A mixture of 4,5-dichloropyrimidine (119 mg, 0.80 mmol), 5-aminoindolin-2-one (119 mg, 0.80 mmol), and TEA (0.133 ml, 0.96 mmol) in DMSO (1.0 mL) was stirred at room temperature for 14 h. The reaction mixture was diluted with a 9:1 mixture of H_2O and EtOH (10 mL). The precipitated solid was collected, washed with H_2O, and dried *in vacuo* to give **6** (95 mg, 46%) as a pale brown solid. ^{1}H NMR (DMSO-d_6) δ 3.49 (2H, s), 6.80 (1H, d, J = 8.2 Hz), 7.25–7.36 (1H, m), 7.40–7.49 (1H, m), 8.39 (1H, s), 8.42 (1H, s), 9.02 (1H, s), 10.36 (1H, s). MS m/z 261.2 $(M+H)^+$. Anal. Calcd for $C_{12}H_9ClN_4O \cdot 0.8\ H_2O$: C, 52.39; H, 3.88; N, 20.37. Found: C, 52.32; H, 4.12; N, 20.30.

5-((5-Chloro-2-((pyridin-3-ylmethyl)amino)pyrimidin-4-yl)amino)-1,3-dihydro-2*H*-indol-2-one (7). A mixture of **16** (120 mg, 0.41 mmol), pyridin-3-ylmethanamine (132 mg, 1.22 mmol), and TEA (49 mg, 0.49 mmol) in DMSO (1.0 mL) was heated at 95 °C for 3 h. The reaction mixture was directly purified by column chromatography (silica gel, eluted with 50% to 100% EtOAc in hexane, followed by 0% to 20% MeOH in EtOAc) to give **7** (34 mg, 22%) as a yellow solid. ^{1}H NMR (DMSO-d_6) δ 3.40 (2H, brs), 4.37 (2H, brs), 6.62–6.77 (1H, m), 7.13–7.71 (5H, m), 7.92 (1H, s), 8.37–8.52 (3H, m), 10.30 (1H, s). MS *m*/*z* 367.0 $(M+H)^+$. Anal. Calcd for $C_{18}H_{15}ClN_6O \cdot 0.1–H_2O \cdot 0.1–EtOAc$: C, 58.56; H, 4.27; N, 22.27. Found: C, 58.40; H, 4.52; N, 22.12. HPLC analysis conditions 1: *R*t = 0.54 min (100% purity); conditions 2: *R*t = 0.80 min (97.3% purity).

2-Chloro-5-fluoro-*N*-phenylpyrimidin-4-amine (14). A mixture of 2,4-dichloro-5-fluoropyrimidine (500 mg, 2.99 mmol), aniline (0.287 ml, 3.14 mmol), and TEA (333 mg, 3.29 mmol) in *i*-PrOH (10 mL) was stirred at room temperature for 3 h. The reaction mixture was diluted with hexane, and the insoluble materials were removed by filtration. The filtrate was concentrated, and the resulting solid was washed with water and dried *in vacuo* to give **14** (530 mg, 79%) as a colorless solid. ^{1}H NMR (DMSO-d_6) δ 7.15 (1H, t, *J* = 7.2 Hz), 7.69 (2H, d, *J* = 8.2 Hz), 8.32 (1H, d, *J* = 3.5 Hz), 9.99 (1H, s). MS *m*/*z* 224.0 $(M+H)^+$.

2,5-Dichloro-*N*-phenylpyrimidin-4-amine (15). A mixture of 2,4,5-trichloropyrimidine (1025 mg, 5.59 mmol), aniline (520 mg, 5.59 mmol), and TEA (565 mg, 5.59 mmol) in *i*-PrOH (20 mL) was heated at reflux for 14 h. The mixture was poured into H_2O and extracted with EtOAc. The organic layer was washed with H_2O and brine, dried over $MgSO_4$, and concentrated *in vacuo*. The residue was purified by column chromatography (silica gel, eluted with 5% to 50%

EtOAc in hexane) to give **15** (900 mg, 67%) as a colorless oil. ^{1}H NMR (DMSO-d_6) δ 7.20 (1H, s), 7.40 (2H, s), 7.58 (2H, d, J = 8.2 Hz), 8.38 (1H, s), 9.52 (1H, s). MS m/z 240.0 $(M+H)^+$.

5-((2,5-Dichloropyrimidin-4-yl)amino)indolin-2-one (16). A mixture of 2,4,5-trichloropyrimidine (0.50 g, 2.73 mmol) and 5-aminoindolin-2-one (0.40 g, 2.73 mmol) in DMSO (1.0 mL) was added with TEA (0.379 ml, 2.73 mmol) at room temperature, and the resultant mixture was stirred at room temperature for 2 h. The resulting solution was diluted with H_2O/EtOH (5:1, 10 mL), and the precipitated solid was collected by filtration. The obtained solid was washed with H_2O and dried *in vacuo* to give **16** (634 mg, 79%) as a pale brown solid. ^{1}H NMR (DMSO-d_6) δ 3.51 (2H, s), 6.82 (1H, d, J = 8.2 Hz), 7.24–7.30 (1H, m), 7.34 (1H, s), 8.31 (1H, s), 9.37–9.49 (1H, m), 10.33–10.51 (1H, m). MS m/z 295.1 $(M+H)^+$.

ASSOCIATED CONTENT

Supporting Information.

The Supporting Information is available free of charge on the ACS Publications website at DOI:

SPR sensorgrams for parallel immobilization, evaluation of stability and DMSO effect, SPR sensorgrams and equilibrium plots for compounds **2**-**6**, electron density OMIT map, data collection and refinement statistics (PDF), molecular formula strings (CSV)

Accession Codes

Atom coordinates and structure factors have been deposited in the Protein Data Bank with accession codes: 5X4M (BCL6/**1**), 5X4N (BCL6/**4**), 5X4O (BCL6/**5**), 5X4P (BCL6/**6**), and

5X4Q (BCL6/**7**). Authors will release the atomic coordinates and experimental data upon article publication.

AUTHOR INFORMATION

Corresponding Authors

*yusuke.kamada1@takeda.com. tel: +81-0466-32-2782; nozomu.sakai@takeda.com. tel: +81-0466-32-1273

ORCID

Y.K.: 0000-0003-3701-2075

Author Contributions

YK and NS contributed equally to this work and wrote most of this paper. YK discovered and analyzed the fragments and their relatives by SPR. NS designed and synthesized the compounds. SS, WL, and GS conducted crystal structure analysis and wrote a part of this paper. KI prepared the recombinant proteins. HO and MI conducted NMR experiments. KS conducted ELISA and M2H assays. YI, JS, and JM supervised and supported this work.

Notes

The authors declared no potential conflicts of interest with respect to the research, authorship, and publication of this article.

ACKNOWLEDGMENT

The authors would like to thank Takamichi Muraki for biochemical experiments, Haihong Wu, Yuuka Hirao, Yoshifumi Nishimura, and Hideaki Shimojo for STD-NMR experiments, Shugo Ohno and Derek Cole for fragment library and compounds supply, and Kengo Okada and Takashi Ito for suggestions, help, and support to this work. We also acknowledge Takeshi Yamamoto, Takeshi Yasui, Takafumi Takai, Yoshihisa Nakada, Takashi Ichikawa, Takayuki Tatamiya, and Masashi Iwata for their kind suggestions. We also thank the staff of the Berkeley Center for Structural Biology who operated the ALS beamlines 5.0.2 and 5.0.3. Berkeley Center for Structural Biology is supported in part by the U.S. National Institutes of Health and U.S. National Institute of General Medical Sciences. The Advanced Light Source is supported by the Director, Office of Science, Office of Basic Energy Sciences of the U.S. Department of Energy under Contract No. DE-AC02-05CH11231.

ABBREVIATIONS

BCL6, B-cell lymphoma 6; BCoR, BCL6 corepressor; SMRT, silencing mediator of retinoic acid and thyroid hormone receptor; NCoR, nuclear receptor corepressor; M2H, mammalian two hybrid assay; Et_3N, triethylamine; EtOAc, ethyl acetate; EtOH, ethanol; IPE, diisopropyl ether; MeCN, acetonitrile; MeOH, methanol; *i*-PrOH, 2-propanol; TEA, triethylamine; TEV, tobacco etch virus; RU, resonance unit.

REFERENCES

(1) Huynh, K. D.; Fischle, W.; Verdin, E.; Bardwell, V. J. BCoR, a novel corepressor involved in BCL-6 repression. *Genes Dev.* **2000**, *14*, 1810-1823.

(2) Dent, A. L.; Shaffer, A. L.; Yu, X.; Allman, D.; Staudt, L. M. Control of inflammation, cytokine expression, and germinal center formation by BCL-6. *Science* **1997**, *276*, 589-592.

(3) Linterman, M. A.; Vinuesa, C. G. Signals that influence T follicular helper cell differentiation and function. *Semin. Immunopathol.* **2010**, *32*, 183-196.

(4) Nurieva, R. I.; Chung, Y.; Martinez, G. J.; Yang, X. O.; Tanaka, S.; Matskevitch, T. D.; Wang, Y. H.; Dong, C. Bcl6 mediates the development of T follicular helper cells. *Science* **2009**, *325*, 1001-1005.

(5) Xin, N.; Fu, L.; Shao, Z.; Guo, M.; Zhang, X.; Zhang, Y.; Dou, C.; Zheng, S.; Shen, X.; Yao, Y.; Wang, J.; Wang, J.; Cui, G.; Liu, Y.; Geng, D.; Xiao, C.; Zhang, Z.; Dong, R. RNA interference targeting Bcl-6 ameliorates experimental autoimmune myasthenia gravis in mice. *Mol. Cell. Neurosci.* **2014**, *58*, 85-94.

(6) Parekh, S.; Prive, G.; Melnick, A. Therapeutic targeting of the BCL6 oncogene for diffuse large B-cell lymphomas. *Leuk. Lymphoma* **2008**, *49*, 874-882.

(7) Duy, C.; Hurtz, C.; Shojaee, S.; Cerchietti, L.; Geng, H.; Swaminathan, S.; Klemm, L.; Kweon, S. M.; Nahar, R.; Braig, M.; Park, E.; Kim, Y. M.; Hofmann, W. K.; Herzog, S.; Jumaa, H.; Koeffler, H. P.; Yu, J. J.; Heisterkamp, N.; Graeber, T. G.; Wu, H.; Ye, B. H.; Melnick, A.; Muschen, M. BCL6 enables Ph+ acute lymphoblastic leukaemia cells to survive BCR-ABL1 kinase inhibition. *Nature* **2011**, *473*, 384-388.

(8) Ahmad, K. F.; Melnick, A.; Lax, S.; Bouchard, D.; Liu, J.; Kiang, C. L.; Mayer, S.; Takahashi, S.; Licht, J. D.; Prive, G. G. Mechanism of SMRT corepressor recruitment by the BCL6 BTB domain. *Mol. Cell* **2003**, *12*, 1551-1564.

(9) Cerchietti, L. C.; Ghetu, A. F.; Zhu, X.; Da Silva, G. F.; Zhong, S.; Matthews, M.; Bunting, K. L.; Polo, J. M.; Fares, C.; Arrowsmith, C. H.; Yang, S. N.; Garcia, M.; Coop, A.;

Mackerell, A. D., Jr.; Prive, G. G.; Melnick, A. A small-molecule inhibitor of BCL6 kills DLBCL cells in vitro and in vivo. *Cancer Cell* **2010**, *17*, 400-411.

(10) Cardenas, M. G.; Yu, W.; Beguelin, W.; Teater, M. R.; Geng, H.; Goldstein, R. L.; Oswald, E.; Hatzi, K.; Yang, S. N.; Cohen, J.; Shaknovich, R.; Vanommeslaeghe, K.; Cheng, H.; Liang, D.; Cho, H. J.; Abbott, J.; Tam, W.; Du, W.; Leonard, J. P.; Elemento, O.; Cerchietti, L.; Cierpicki, T.; Xue, F.; MacKerell, A. D., Jr.; Melnick, A. M. Rationally designed BCL6 inhibitors target activated B cell diffuse large B cell lymphoma. *J. Clin. Invest.* **2016**, *126*, 3351-3362.

(11) Cerchietti, L. C.; Yang, S. N.; Shaknovich, R.; Hatzi, K.; Polo, J. M.; Chadburn, A.; Dowdy, S. F.; Melnick, A. A peptomimetic inhibitor of BCL6 with potent antilymphoma effects in vitro and in vivo. *Blood* **2009**, *113*, 3397-3405.

(12) Evans, S. E.; Goult, B. T.; Fairall, L.; Jamieson, A. G.; Ko Ferrigno, P.; Ford, R.; Schwabe, J. W.; Wagner, S. D. The ansamycin antibiotic, rifamycin SV, inhibits BCL6 transcriptional repression and forms a complex with the BCL6-BTB/POZ domain. *PLoS One* **2014**, *9*, e90889.

(13) Sakamoto, K.; Sogabe, S.; Kamada, Y.; Sakai, N.; Asano, K.; Yoshimatsu, M.; Ida, K.; Imaeda, Y.; Sakamoto, J. I. Discovery of high-affinity BCL6-binding peptide and its structure-activity relationship. *Biochem. Biophys. Res. Commun.* **2017**, *482*, 310-316.

(14) Erlanson, D. A.; Fesik, S. W.; Hubbard, R. E.; Jahnke, W.; Jhoti, H. Twenty years on: the impact of fragments on drug discovery. *Nat. Rev. Drug Discovery* **2016**, *15*, 605-619.

(15) Ludlow, R. F.; Verdonk, M. L.; Saini, H. K.; Tickle, I. J.; Jhoti, H. Detection of secondary binding sites in proteins using fragment screening. *Proc. Natl. Acad. Sci. U. S. A.* **2015**, *112*, 15910-15915.

(16) Jordan, J. B.; Whittington, D. A.; Bartberger, M. D.; Sickmier, E. A.; Chen, K.; Cheng, Y.; Judd, T. Fragment-linking approach using (19)F NMR spectroscopy to obtain highly potent and selective inhibitors of beta-secretase. *J. Med. Chem.* **2016**, *59*, 3732-3749.

(17) Kohlmann, A.; Zech, S. G.; Li, F.; Zhou, T.; Squillace, R. M.; Commodore, L.; Greenfield, M. T.; Lu, X.; Miller, D. P.; Huang, W. S.; Qi, J.; Thomas, R. M.; Wang, Y.; Zhang, S.; Dodd, R.; Liu, S.; Xu, R.; Xu, Y.; Miret, J. J.; Rivera, V.; Clackson, T.; Shakespeare, W. C.; Zhu, X.; Dalgarno, D. C. Fragment growing and linking lead to novel nanomolar lactate dehydrogenase inhibitors. *J. Med. Chem.* **2013**, *56*, 1023-1040.

(18) Larsson, E. A.; Jansson, A.; Ng, F. M.; Then, S. W.; Panicker, R.; Liu, B.; Sangthongpitag, K.; Pendharkar, V.; Tai, S. J.; Hill, J.; Dan, C.; Ho, S. Y.; Cheong, W. W.; Poulsen, A.; Blanchard, S.; Lin, G. R.; Alam, J.; Keller, T. H.; Nordlund, P. Fragment-based ligand design of novel potent inhibitors of tankyrases. *J. Med. Chem.* **2013**, *56*, 4497-4508.

(19) Wielens, J.; Headey, S. J.; Rhodes, D. I.; Mulder, R. J.; Dolezal, O.; Deadman, J. J.; Newman, J.; Chalmers, D. K.; Parker, M. W.; Peat, T. S.; Scanlon, M. J. Parallel screening of low molecular weight fragment libraries: do differences in methodology affect hit identification? *J. Biomol. Screening* **2013**, *18*, 147-159.

(20) Giannetti, A. M.; Koch, B. D.; Browner, M. F. Surface plasmon resonance based assay for the detection and characterization of promiscuous inhibitors. *J. Med. Chem.* **2008**, *51*, 574-580.

(21) Retra, K.; Irth, H.; van Muijlwijk-Koezen, J. E. Surface plasmon resonance biosensor analysis as a useful tool in FBDD. *Drug Discovery Today: Technol.* **2010**, *7*, e181-e187.

(22) Chimenti, M. S.; Bulfer, S. L.; Neitz, R. J.; Renslo, A. R.; Jacobson, M. P.; James, T. L.; Arkin, M. R.; Kelly, M. J. A fragment-based ligand screen against part of a large protein machine: the ND1 domains of the AAA+ ATPase p97/VCP. *J. Biomol. Screening* **2015**, *20*, 788-800.

(23) Giannetti, A. M.; Zheng, X.; Skelton, N. J.; Wang, W.; Bravo, B. J.; Bair, K. W.; Baumeister, T.; Cheng, E.; Crocker, L.; Feng, Y.; Gunzner-Toste, J.; Ho, Y. C.; Hua, R.; Liederer, B. M.; Liu, Y.; Ma, X.; O'Brien, T.; Oeh, J.; Sampath, D.; Shen, Y.; Wang, C.; Wang, L.; Wu, H.; Xiao, Y.; Yuen, P. W.; Zak, M.; Zhao, G.; Zhao, Q.; Dragovich, P. S. Fragment-based identification of amides derived from trans-2-(pyridin-3-yl)cyclopropanecarboxylic acid as potent inhibitors of human nicotinamide phosphoribosyltransferase (NAMPT). *J. Med. Chem.* **2014**, *57*, 770-792.

(24) Hendrick, A. G.; Muller, I.; Willems, H.; Leonard, P. M.; Irving, S.; Davenport, R.; Ito, T.; Reeves, J.; Wright, S.; Allen, V.; Wilkinson, S.; Heffron, H.; Bazin, R.; Turney, J.; Mitchell, P. J. Identification and investigation of novel binding fragments in the fatty acid binding protein 6 (FABP6). *J. Med. Chem.* **2016**, *59*, 8094-8102.

(25) Lund, B. A.; Christopeit, T.; Guttormsen, Y.; Bayer, A.; Leiros, H. K. Screening and design of inhibitor scaffolds for the antibiotic resistance oxacillinase-48 (OXA-48) through surface plasmon resonance screening. *J. Med. Chem.* **2016**, *59*, 5542-5554.

(26) Davies, T. G.; Wixted, W. E.; Coyle, J. E.; Griffiths-Jones, C.; Hearn, K.; McMenamin, R.; Norton, D.; Rich, S. J.; Richardson, C.; Saxty, G.; Willems, H. M.; Woolford, A. J.; Cottom, J. E.; Kou, J. P.; Yonchuk, J. G.; Feldser, H. G.; Sanchez, Y.; Foley, J. P.; Bolognese, B. J.; Logan, G.; Podolin, P. L.; Yan, H.; Callahan, J. F.; Heightman, T. D.; Kerns, J. K. Monoacidic inhibitors of the kelch-like ECH-associated protein 1: nuclear factor erythroid 2-related factor 2 (KEAP1:NRF2) protein-protein interaction with high cell potency identified by fragment-based discovery. *J. Med. Chem.* **2016**, *59*, 3991-4006.

(27) F. Bower, J.; Pannifer, A. Using fragment-based technologies to target protein-protein interactions. *Curr. Pharm. Des.* **2012**, *18*, 4685-4696.

(28) Wartchow, C. A.; Podlaski, F.; Li, S.; Rowan, K.; Zhang, X.; Mark, D.; Huang, K. S. Biosensor-based small molecule fragment screening with biolayer interferometry. *J. Comput.-Aided Mol. Des.* **2011**, *25*, 669-676.

(29) Yoshimura, C.; Miyafusa, T.; Tsumoto, K. Identification of small-molecule inhibitors of the human S100B-p53 interaction and evaluation of their activity in human melanoma cells. *Bioorg. Med. Chem.* **2013**, *21*, 1109-1115.

(30) Whittaker, M. Picking up the pieces with FBDD or FADD: invest early for future success. *Drug Discovery Today* **2009**, *14*, 623-624.

(31) Varnes, J. G.; Geschwindner, S.; Holmquist, C. R.; Forst, J.; Wang, X.; Dekker, N.; Scott, C. W.; Tian, G.; Wood, M. W.; Albert, J. S. Fragment-assisted hit investigation involving integrated HTS and fragment screening: Application to the identification of phosphodiesterase 10A (PDE10A) inhibitors. *Bioorg. Med. Chem. Lett.* **2016**, *26*, 197-202.

(32) Elinder, M.; Geitmann, M.; Gossas, T.; Kallblad, P.; Winquist, J.; Nordstrom, H.; Hamalainen, M.; Danielson, U. H. Experimental validation of a fragment library for lead discovery using SPR biosensor technology. *J. Biomol. Screening* **2011**, *16*, 15-25.

(33) Hamalainen, M. D.; Zhukov, A.; Ivarsson, M.; Fex, T.; Gottfries, J.; Karlsson, R.; Bjorsne, M. Label-free primary screening and affinity ranking of fragment libraries using parallel analysis of protein panels. *J. Biomol. Screening* **2008**, *13*, 202-209.

(34) Nordstrom, H.; Gossas, T.; Hamalainen, M.; Kallblad, P.; Nystrom, S.; Wallberg, H.; Danielson, U. H. Identification of MMP-12 inhibitors by using biosensor-based screening of a fragment library. *J. Med. Chem.* **2008**, *51*, 3449-3459.

(35) Navratilova, I.; Macdonald, G.; Robinson, C.; Hughes, S.; Mathias, J.; Phillips, C.; Cook, A. Biosensor-based approach to the identification of protein kinase ligands with dual-site modes of action. *J. Biomol. Screening* **2012**, *17*, 183-193.

(36) Nordin, H.; Jungnelius, M.; Karlsson, R.; Karlsson, O. P. Kinetic studies of small molecule interactions with protein kinases using biosensor technology. *Anal. Biochem.* **2005**, *340*, 359-368.

(37) Stenlund, P.; Frostell-Karlsson, A.; Karlsson, O. P. Studies of small molecule interactions with protein phosphatases using biosensor technology. *Anal. Biochem.* **2006**, *353*, 217-225.

(38) Hopkins, A. L.; Groom, C. R.; Alex, A. Ligand efficiency: a useful metric for lead selection. *Drug Discovery Today* **2004**, *9*, 430-431.

(39) Hopkins, A. L.; Keseru, G. M.; Leeson, P. D.; Rees, D. C.; Reynolds, C. H. The role of ligand efficiency metrics in drug discovery. *Nat. Rev. Drug Discovery* **2014**, *13*, 105-121.

(40) Perspicace, S.; Banner, D.; Benz, J.; Muller, F.; Schlatter, D.; Huber, W. Fragment-based screening using surface plasmon resonance technology. *J. Biomol. Screening* **2009**, *14*, 337-349.

(41) Otwinowski, Z.; Minor, W. Processing of X-ray diffraction data collected in oscillation mode. In *Macromolecular Crystallography, part A*, Carter, C. W. J.; Sweet, R. M., Eds. Academic Press: New York, 1997; Vol. 276, pp. 307-326.

(42) Vagin, A.; Teplyakov, A. MOLREP: An automated program for molecular replacement. *J. Appl. Crystallogr.* **1997**, *30*, 1022-1025.

(43) Collaborative Computational Project, N. The CCP4 suite: programs for protein crystallography. *Acta Crystallogr., Sect. D: Biol. Crystallogr.* **1994**, *50*, 760-763.

(44) Murshudov, G. N.; Skubak, P.; Lebedev, A. A.; Pannu, N. S.; Steiner, R. A.; Nicholls, R. A.; Winn, M. D.; Long, F.; Vagin, A. A. REFMAC5 for the refinement of macromolecular crystal structures. *Acta Crystallogr., Sect. D: Biol. Crystallogr.* **2011**, *67*, 355-367.

(45) Emsley, P.; Lohkamp, B.; Scott, W. G.; Cowtan, K. Features and development of Coot. *Acta Crystallogr., Sect. D: Biol. Crystallogr.* **2010**, *66*, 486-501.

(46) Chen, V. B.; Arendall, W. B., 3rd; Headd, J. J.; Keedy, D. A.; Immormino, R. M.; Kapral, G. J.; Murray, L. W.; Richardson, J. S.; Richardson, D. C. MolProbity: all-atom structure

validation for macromolecular crystallography. *Acta Crystallogr., Sect. D: Biol. Crystallogr.* **2010**, *66*, 12-21.

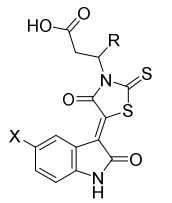

79-6: R = CO_2H, X = Br
K_D = 129 μM[a]
FX1: R = H, X = Cl
K_D = 7 μM[a]

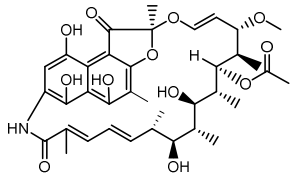

Rifamycin SV
K_D = ~ 1 mM[b]

Ac-LWYTDIRMSWRVP-OH

F1324
K_D = 0.57 nM[c]

TAT-GRGIEHISR-Fu[d]

RI-BPI
GI_{50} = ~10 μM[e]

Figure 1. Known BCL6 inhibitors. [a] Determined by microscale thermophoresis.[10] [b] Determined by Fluorescence polarization assay.[12] [c] Determined by SPR.[13] [d] all D-amino acids, TAT means cell penetrating peptide sequence, Fu means fusogenic peptide sequence.[11] [e] Determined by DLBCL cell growth inhibition.[11]

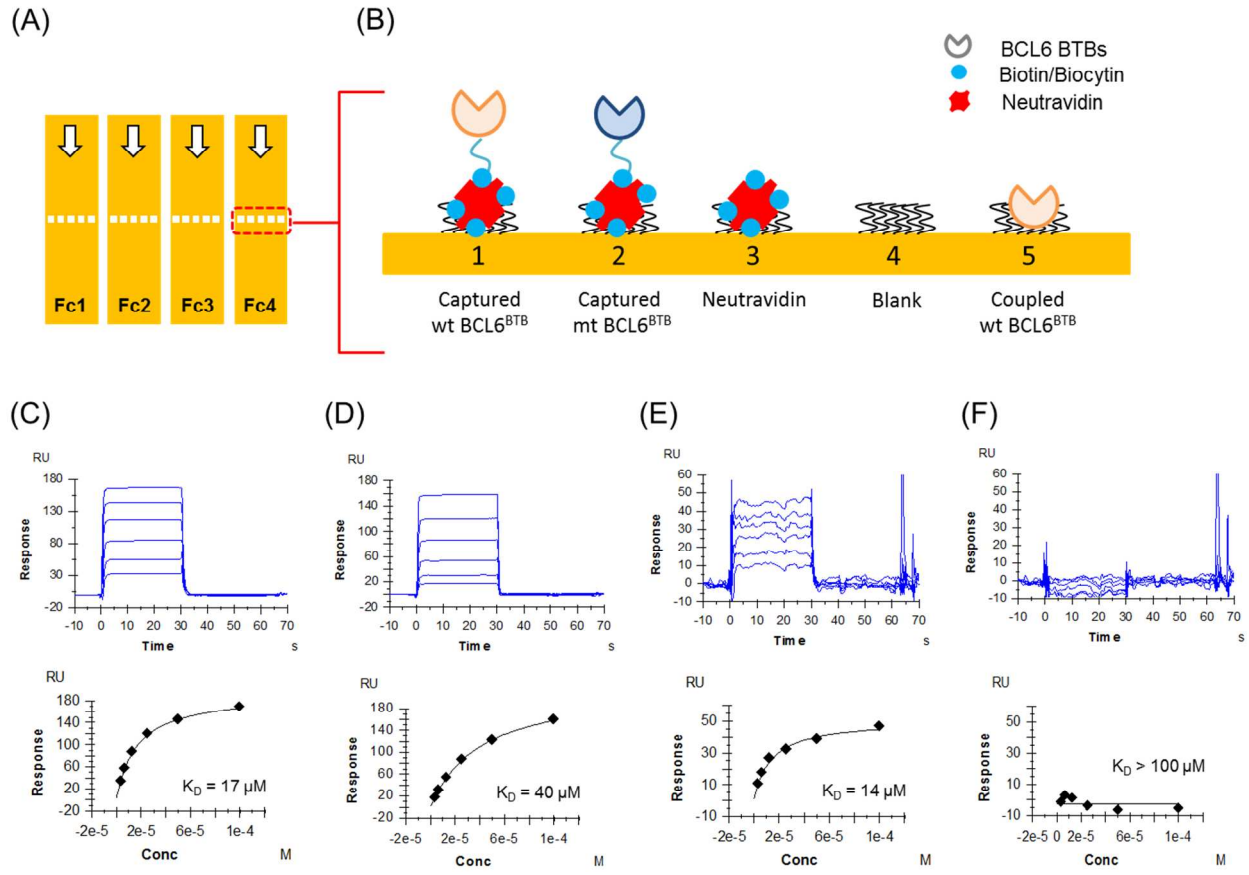

Figure 2. Layout of the sensor chip. (A) Four independent flow cells (Fc), each with five detection spots. (B) Protein immobilized in each flow cell. Binding responses of captured wt BCL6^{BTB}, captured mt BCL6^{BTB}, coupled wt BCL6^{BTB}, and NeutrAvidin are detected on spots 1–3, spots 2–3, spots 5–4, and spots 3–4, respectively. Sensorgrams of BCoR peptide binding to (C) captured wt BCL6^{BTB}, (D) captured mt BCL6^{BTB}, (E) coupled wt BCL6^{BTB}, and (F) NeutrAvidin. Lower graphs indicate the fit plots of the response measured at equilibrium plotted against BCoR peptide concentration. Top concentration is 100 µM; dilution step is two-fold.

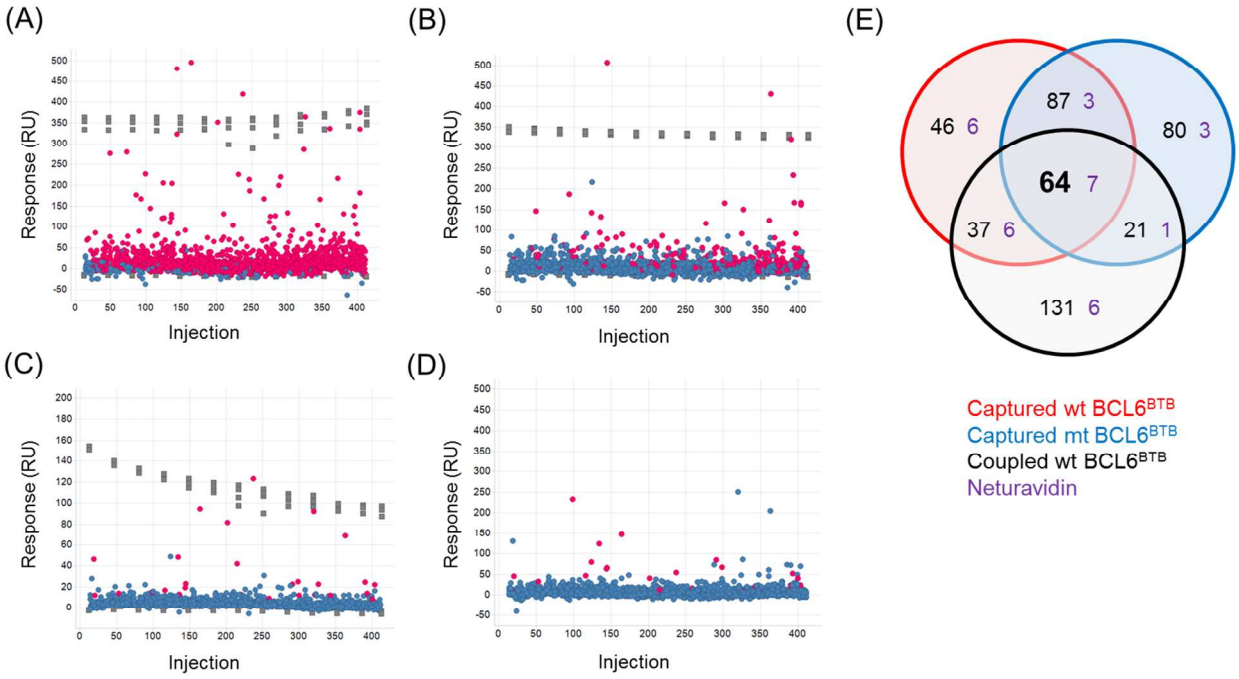

Figure 3. SPR-based screening of 1494 fragments tested against (A) captured wt $BCL6^{BTB}$, (B) captured mt $BCL6^{BTB}$, (C) coupled wt $BCL6^{BTB}$, and (D) NeutrAvidin. The color of each plot indicates fast binding (blue-circle), slow binding (red-circle), and 100 μM BCoR peptide as a positive control (gray-square). (E) Venn diagram showing the number of fragments selected at each $BCL6^{BTB}$ screening and the overlap of fragments found by each screening.

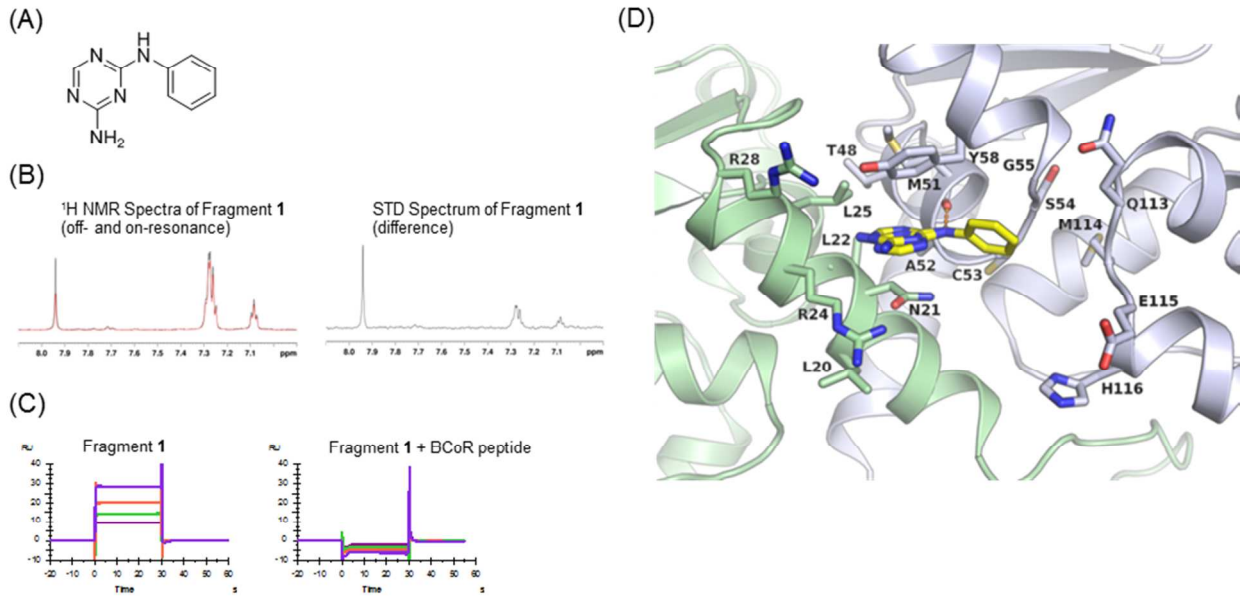

Figure 4. Characterization of fragment **1**. (A) Chemical structure of fragment **1**. (B) STD-NMR experiments. ^{1}H spectra of fragment **1** for off-resonance (black line) and on-resonance (red line), and the STD spectrum of fragment **1** (difference). (C) SPR competition experiments. Sensorgrams of fragment **1** to mt BCL6^{BTB} in the absence or presence of 100 μM BCoR peptide. Top concentration is 1 mM; dilution step is two-fold. (D) Co-crystal structure of fragment **1** in complex with BCL6^{BTB}.

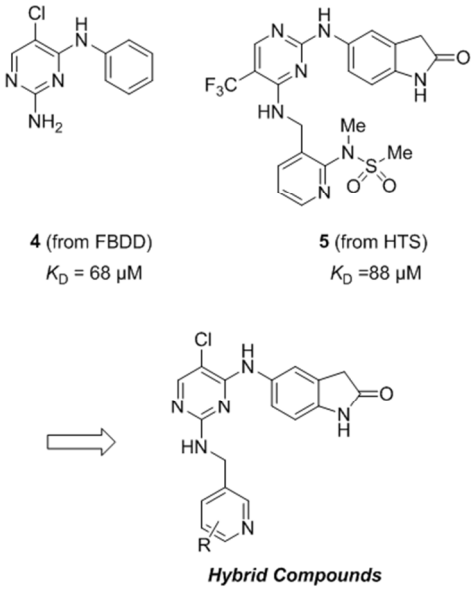

Figure 5. Consolidation of the fragment-based inhibitor **4** with hit compound **5**.

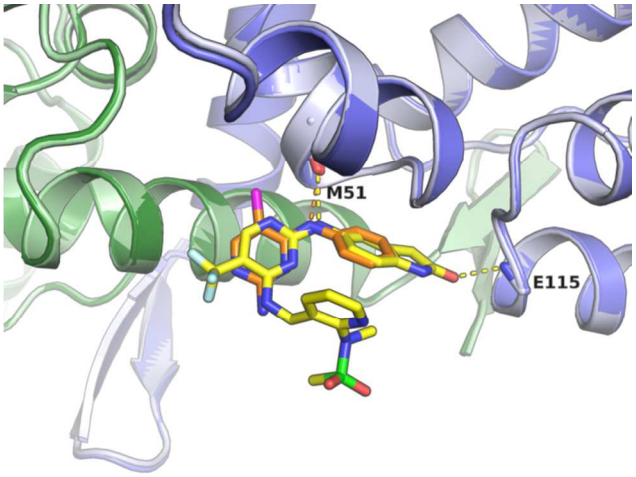

Figure 6. Structural superposition of the complex structures with compounds **4** (orange) and **5** (yellow).

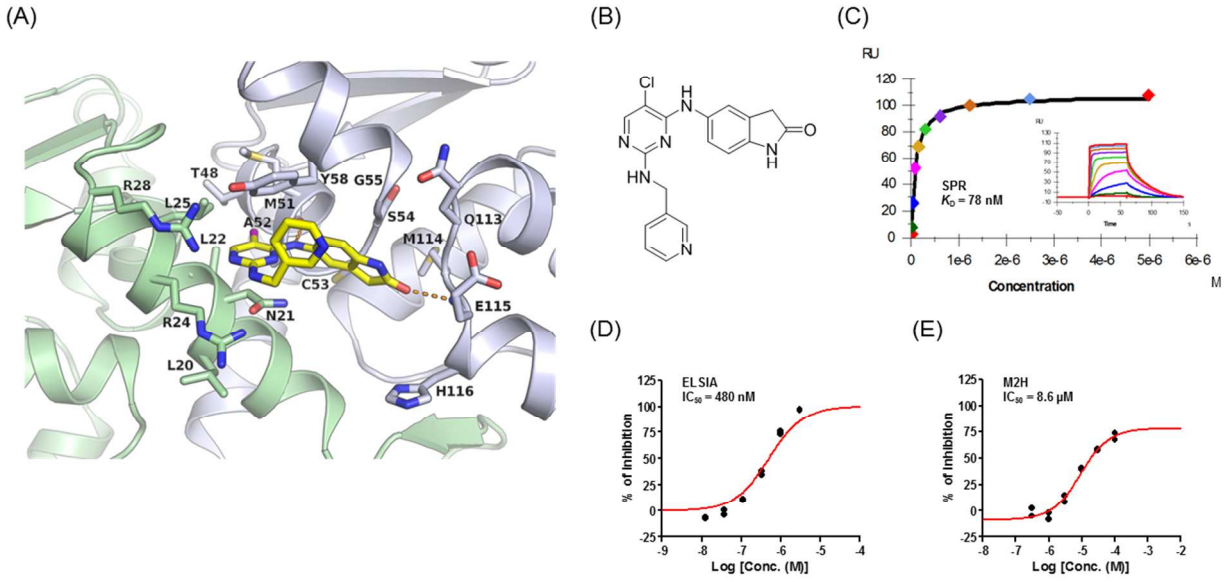

Figure 7. (A) Co-crystal structure of compound **7** in complex with $BCL6^{BTB}$. (B) Chemical structure of **7**. (C) Equilibrium plot and sensorgrams (insert) of **7** binding to BCL6. (D, E) PPI inhibitory activities in cell-free (ELISA) and cellular (M2H) assays.

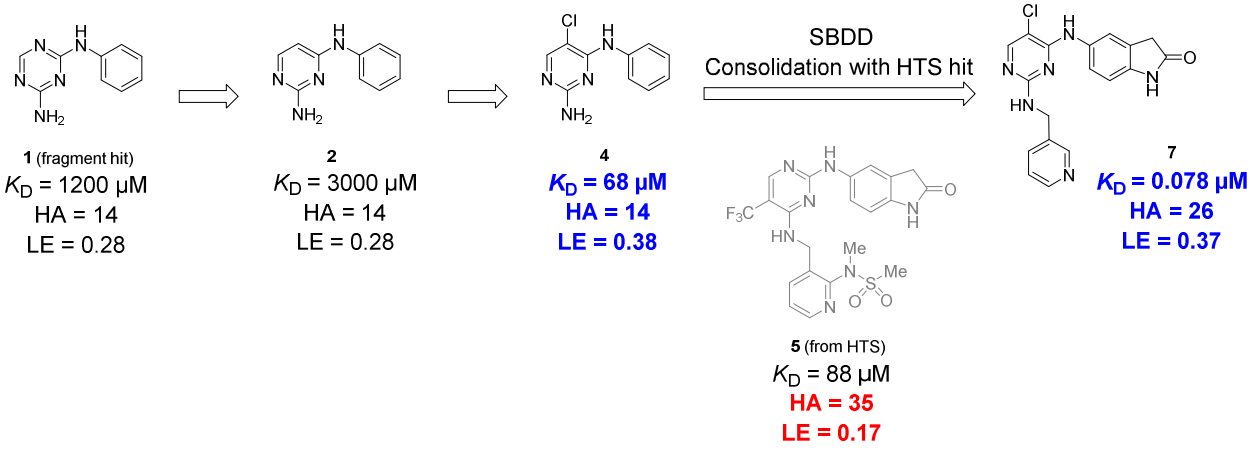

Figure 8. Summary of the FBDD approach for identification of the compound **7**.

Table 1. Binding affinities between BCoR peptide and $BCL6^{BTB}$s

DMSO	wt $BCL6^{BTB}$		mt $BCL6^{BTB}$	
	K_D (μM)	R_{max} (RU)	K_D (μM)	R_{max} (RU)
1%	7.5	245	17	311
3%	9.3	242	21	302
5%	12	243	25	304

Table 2. Structure-activity relationships of the pyrimidine derivatives

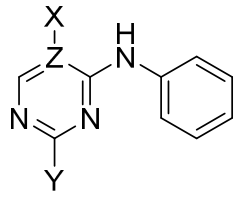

compd	X	Y	Z	K_D [a] (μM)	LE
1	-	NH_2	N	1200	0.28
2	H	NH_2	C	3000	0.25
3	F	NH_2	C	180	0.34
4	Cl	NH_2	C	68	0.38

[a] K_D values are reported as the arithmetic mean of at least two separate runs (n = 2).

Table 3. BCL6 binding affinities of the hybrid-type compounds

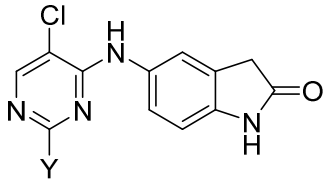

compd	Y	K_D [a] (μM)	LE
6	H	9.3	0.38
7	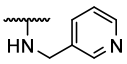	0.078	0.37

[a] K_D values are reported as the arithmetic mean of at least two separate runs (n = 2).

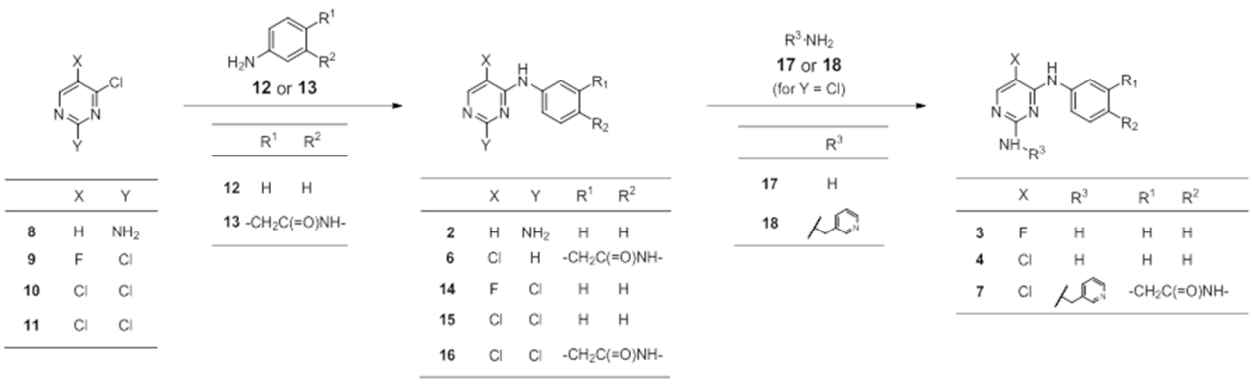

	X	Y
8	H	NH_2
9	F	Cl
10	Cl	Cl
11	Cl	Cl

	R^1	R^2
12	H	H
13	$-CH_2C(=O)NH-$	

	X	Y	R^1	R^2
2	H	NH_2	H	H
6	Cl	H	$-CH_2C(=O)NH-$	
14	F	Cl	H	H
15	Cl	Cl	H	H
16	Cl	Cl	$-CH_2C(=O)NH-$	

	R^3
17	H
18	

	X	R^3	R^1	R^2
3	F	H	H	H
4	Cl	H	H	H
7	Cl		$-CH_2C(=O)NH-$	

Scheme 1. General synthetic procedure for the pyrimidine derivatives

Table of Contents graphic